Review of Scientific Instruments ARTICLE scitation.org/journal/rsi

High precision, low excitation capacitance measurement methods from 10 mK to room temperature

Cite as: Rev. Sci. Instrum. 93, 053910 (2022); doi: 10.1063/5.0087772
Submitted: 9 February 2022 • Accepted: 30 April 2022 •
Published Online: 20 May 2022

Lili Zhao,[1] Wenlu Lin,[1] Xing Fan,[2] Yuanjun Song,[3] Hong Lu,[2,a)] and Yang Liu[1,a)]

AFFILIATIONS

[1] International Center for Quantum Materials, Peking University, Beijing 100871, China
[2] College of Engineering and Applied Sciences, Nanjing University, Nanjing 210093, China
[3] Beijing Academy of Quantum Information Sciences, Beijing 100193, China

[a)] **Authors to whom correspondence should be addressed:** hlu@nju.edu.cn and liuyang02@pku.edu.cn

ABSTRACT

Capacitance measurement is a useful technique in studying quantum devices, as it directly probes the local particle charging properties, i.e., the system compressibility. Here, we report one approach that can measure capacitance from mK to room temperature with excellent accuracy. Our experiments show that such a high-precision technique is able to reveal delicate and essential properties of high-mobility two-dimensional electron systems.

I. INTRODUCTION

Capacitance contains useful information of electronic devices, as it directly probes their electrical charging properties.[1–7] Recently, the capacitance measurement at cryogenic temperature has attracted significant attention in quantum studies and has revealed a series of quantum phenomena.[8–16] Although high precision capacitance measurement is widely used in studying classical devices, such as field effect transistors and diodes, it is extremely difficult to be performed on quantum devices. First, the quantum phenomena usually emerge in fragile systems so that the excitation should be sufficiently low to preserve the quantum properties of the device. Second, many quantum devices can only be studied in cryostats that host the low temperature and high magnetic field environment. The meter-long cables connecting samples and room temperature instruments have ~100 pF capacitance, which is orders-of-magnitude larger than the devices themselves. Third, the total power dissipation at the cryogenic sample stage must be limited to sub-μW in order to maintain the low-temperature environment. This limits the use of active devices.

In order to reduce the crosstalk and signal leaking between cables, many reported works use the cryogenic preamplifier to isolate the input and output signals.[5,10,11,17,18] Unfortunately, the preamplifiers usually dissipate more than ~10 μW heat at the sample stage, which is sufficiently high to cause a noticeable temperature raise. Sometimes, indirect probes of capacitance, such as penetration field, are used, which can provide qualitative information about quantum phase transitions.[7,12–15]

In this report, we introduce a new approach for high precision capacitance measurement from 10 mK to room temperature. We install a passive bridge at the sample stage and use a voltage-controlled-variable-resistance to *in situ* tune its balance. We use radio frequency excitation to increase the output signal and develop a high sensitivity radio frequency (RF) lock-in technique to analyze the bridge output.

II. METHOD

The passive bridge at the sample stage [Fig. 1(a)] consists of the device under test C_{DUT}, the reference capacitor C_{ref}, the reference resistor R_{ref}, and a voltage-controlled-variable-resistor R_h. R_{ref} is a 51 Ω metal-film resistor whose resistance remains constant from room temperature down to ~10 mK. R_h is the drain-to-source resistance of a high electron mobility transistor (HEMT, model ATF35143). The typical R_h dependence on its the gate voltage V_h at 10 mK is shown in the inset of Fig. 1(b). The excitation voltage

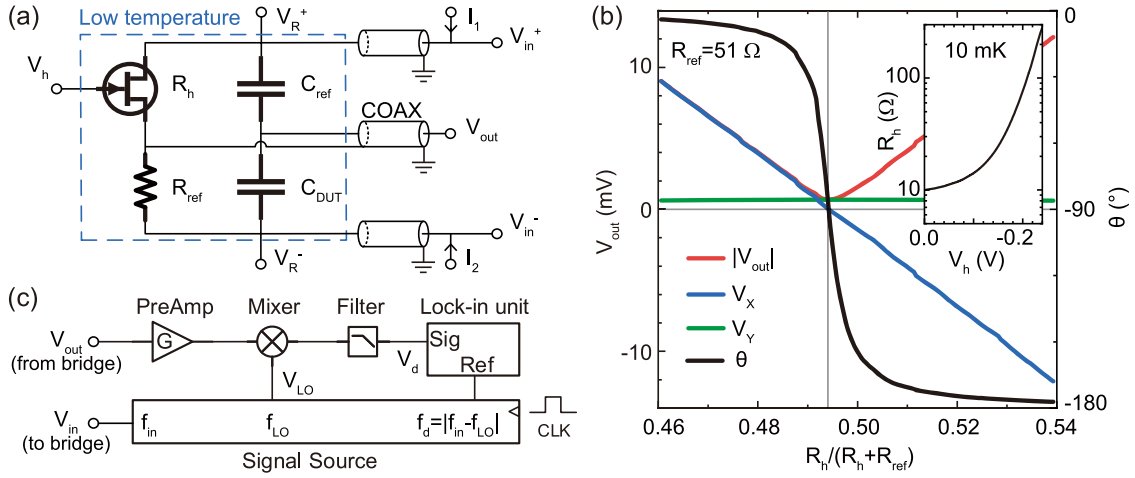

FIG. 1. Schematic diagram of our measurement setup. (a) The passive capacitance bridge installed at the sample stage consists C_{DUT}, C_{ref}, R_{ref}, and R_h. R_h can be tuned by V_h. V_{in}^+ and V_{in}^- are the two differentially coupled input signals, and V_{out} is the output signal. Coaxial cables are used to improve the transmission efficiency and minimize the parasitic capacitance. I_1 and I_2 are two quasi-DC current inputs with different frequencies, and R_h (R_{ref}) can be deduced by analyzing the frequency component same as I_1 (I_2) of the differential voltage between V_R^+ and V_R^-. (b) One typical result of the "V-curve" procedure. The cross point is the balance point of the bridge, signaled by the $|V_{out}|$ minimum, and C_{DUT} can be calculated using Eq. (1). V_{out} can be decomposed into V_y and V_x. $V_x = 0$ at the balancing point and depends on $\frac{R_h}{R_{ref}+R_h}$ linearly. The inset is a typical R_h vs V_h at 10 mK. (c) Diagram of the radio-frequency lock-in setup. The bridge output V_{out} passes through a room-temperature amplifier (PreAmp), a mixer (Mixer), and a low-pass filter (Filter) and turns into a low frequency signal V_d whose frequency is $f_d = |f_{in} - f_{LO}|$. V_d is then analyzed by an audio-frequency digital lock-in unit.

V_{in} is differentially coupled to the V_{in}^+ and V_{in}^- ports of the bridge by a RF transformer, and the output signal V_{out} is the voltage difference between the midpoints of the capacitor and resistor arms. The bridge dissipates only ~10 nW when $V_{in} \simeq 1$ mV_{rms}, mostly caused by R_{ref} and R_h.

We can tune the balance of the bridge by adjusting R_h. The bridge reaches its balance point when the balance condition

$$\frac{C_{DUT}}{C_{ref}} = \frac{R_h}{R_{ref}} \tag{1}$$

is achieved, signaled by the $|V_{out}|$ minimum [see Fig. 1(b)]. Two low-frequency current inputs I_1 and I_2 are injected into the bridge. They flow into the ground through R_h and R_{ref}, respectively, and generate a voltage difference $(V_R^+ - V_R^-) = I_1 \cdot R_h - I_2 \cdot R_{ref}$. We can *in situ* measure R_h and R_{ref} simultaneously with the lock-in technique by locking the frequency of $(V_R^+ - V_R^-)$ to be the same as I_1 and I_2, respectively. Therefore, as long as C_{ref} is stable, the absolute value of C_{DUT} can be deduced by Eq. (1). The $|V_{out}|$ vs R_h curve is "V"-shaped, so we call this procedure as the "V-curve" procedure for brevity.

The output impedance of this bridge is about $\frac{1}{2\pi f(C_{ref}+C_{DUT})}$, where f is the frequency of V_{in}. C_{DUT} and C_{ref} are typically in the order of 0.1 pF, corresponding to output impedance as large as ~1 GΩ when f = 1 kHz. Therefore, we increase f to ~100 MHz so that the output impedance decreases to about 10 kΩ. We use the ~3 m long 50 Ω-characteristic-impedance coaxial cable to connect the bridge and the room-temperature preamplifier, which has a 50 Ω-input-impedance in order to minimize the frequency-dependence. When the excitation amplitude is $\simeq 1 mV_{rms}$, V_{out} is only about ~1 μV_{rms}, and the 0.1% change in C_{DUT} corresponds to $\simeq 1$ nV_{rms} variation in the output. In order to analyze such a small signal, we combine the superheterodyne and lock-in techniques [see Fig. 1(c)]. The signal source generates three single-frequency signals V_{in}, V_{LO}, and V_{ref} with frequencies f_{in}, f_{LO}, and f_d, respectively, where $f_d = |f_{in} - f_{LO}|$. V_{in} is sent to the bridge as the voltage excitation. The bridge output V_{out} passes through a room-temperature preamplifier, a mixer, and a low-pass filter and turns into a low frequency signal V_d. We use a digital audio-frequency lock-in unit to measure the amplitude $|V_d|$ and phase θ_d in reference to V_{ref}, where $|V_d| \propto |V_{out}|$ and θ_d is the same as the phase difference between V_{out} and V_{in} but differs by a constant. For simplicity, we quote $|V_d|$ and θ_d as the amplitude $|V_{out}|$ and the (relative) phase θ (from V_{in}) of the bridge output.

III. CALIBRATION

We calibrate our setup at room temperature by measuring fixed-value capacitors whose nominal value C_{nom} ranges from 0.1 to 10 pF [see Fig. 2(a)]. We select different C_{ref} that is comparable with C_{DUT}. The y-axis is the measured C_{DUT} using the "V-curve" procedure with ≃1.5 mV_{rms} excitation amplitude and ≃ 110 MHz frequency. The horizontal and vertical error bars are deduced from the tolerance of C_{DUT} and C_{ref}, which dominate the inaccuracy at <1 pF.

The measured C_{DUT} matches its nominal value C_{nom} even for capacitors as small as 0.1 pF, evidencing that our setup is capable of measuring the absolute capacitance value with an accuracy about 0.1 pF.[19] In addition, there is deviation between the resistance value measured at low frequency and that at high frequency due to the existence of parasitic capacitance in parallel with both R_h and R_{ref}.

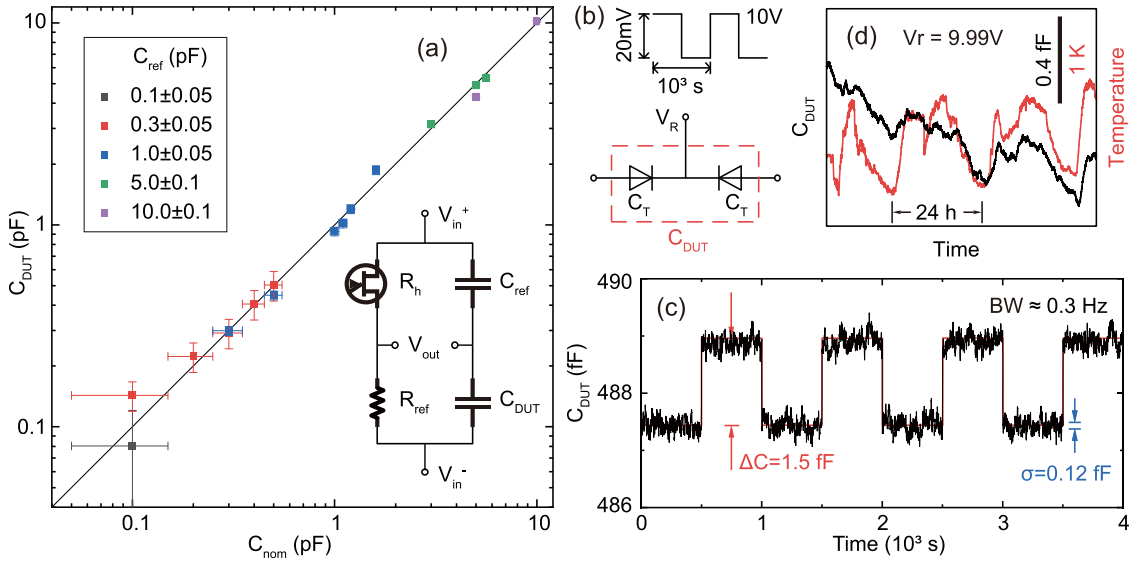

FIG. 2. Room temperature examination of our setup. (a) C_{DUT} is the measured capacitor values using the "V-curve" procedure. C_{nom} is their nominal value given by manufacturers, and the error bar is deduced from their tolerance. The black line is the ideal $C_{DUT} = C_{nom}$. Different colors of point data represent different C_{ref} used. (b) Measuring two tunable capacitance diodes in series. The reverse voltage V_R tunes the value of each diode capacitance C_T. V_R is a 1000-second-period, square wave with high/low voltages equal 10/9.98 V. (c) Measured C_{DUT}. $C_{DUT} \approx 487.5$ fF for $V_R = 10$ V and increases by 1.5 fF when V_R decreases by 20 mV. The standard deviation is as low as 0.1 fF at 0.3 Hz measurement bandwidth. (d) Long period monitoring of C_{DUT} with V_R fixed at 9.99 V (black), as well as the room temperature (red).

This deviation becomes larger as f_{in} increases but is <1% at our typical capacitance measurement frequency, i.e., $f_{in} = 100$ MHz. In addition, R_h has a frequency dependence that originates from the finite electron scattering time in the channel, which we have no precise evaluation. Fortunately, from the fact that measured capacitance is nearly the same of the calibration capacitance in Fig. 2(a), we believe that such a discrepancy is sufficiently small.

The "V-curve" procedure can measure the absolute value of C_{DUT} with decent accuracy; however, continuously monitoring C_{DUT} while sweeping particular physical parameters, such as magnetic field and temperature, is of more interest. We can deduce C_{DUT} from V_{out} using the V_{out} vs R_h relation obtained by the "V-curve" procedure. At the vicinity of the balance point, the bridge output V_{out} is approximately[20]

$$V_{out} \propto \left(\frac{C_{DUT}}{C_{ref} + C_{DUT}} - \frac{R_h}{R_{ref} + R_h} \right) \cdot V_{in} + V_0, \tag{2}$$

where V_0 represents the leaking signal. V_{out} is a vector and can be decomposed into two orthogonal scalar components using its amplitude $|V_{out}|$ and phase θ,

$$\begin{cases} V_x = |V_{out}| \cdot \cos(\theta), \\ V_y = |V_{out}| \cdot \sin(\theta). \end{cases} \tag{3}$$

Note that in the ideal case when $V_0 = 0$, V_{out} changes its sign or θ changes by 180° as we tune the bridge through its balance point. We set $\theta = -90°$ at the balance point so that $V_x = V_{out}$ is the expected bridge output [Fig. 1(b)]. In a careful measurement, leaking signal V_0 mostly comes from the capacitive coupling between the input and output cables and has a 90° phase shift from V_{in}.

At the vicinity of the balance point, $V_y \approx V_0$ and V_x has a linear dependence on $\frac{R_h}{R_{ref}+R_h}$; see Fig. 1(b). From the symmetry between the resistors and capacitors in the bridge, we assume that a single parameter, the sensitivity S, can describe the dependence of V_x on both R_h and C_{DUT} by

$$S = \frac{\partial V_x}{\partial \frac{R_h}{R_{ref}+R_h}} = -\frac{\partial V_x}{\partial \frac{C_{DUT}}{C_{ref}+C_{DUT}}}. \tag{4}$$

S can be obtained by linearly fitting V_x with $\frac{R_h}{R_{ref}+R_h}$ while keeping C_{DUT} fixed. Note that S is inversely proportional to the output impedance $1/2\pi f(C_{ref} + C_{DUT})$, and the corresponding corrections might be necessary.[20] Thereafter, we can deduce C_{DUT} from V_{out} by

$$\frac{C_{DUT}}{C_{ref} + C_{DUT}} = \frac{R_h}{R_{ref} + R_h} - \frac{V_x}{S} \tag{5}$$

at the vicinity of the balance point.

Figures 2(b)–2(d) examine the feasibleness of the "monitoring"-mode. The device-under-test is two back-to-back connected tunable capacitance diodes (Infineon BB837) whose capacitance C_T can be controlled by its reverse bias voltage V_R. V_R has a 9.99 V DC component that biases $C_{DUT} = 0.5C_T$ to about 500 fF, as well as a 20 mV_{pp}, 1000-second-period square-wave AC component that induces a small capacitance variation; see Fig. 2(b). The frequency and amplitude of V_{in} are 110 MHz and ~1 mV_{rms}, respectively. We show the measured capacitance using the "monitoring"-mode in Fig. 2(c). The measured C_{DUT} is about 487.5 fF when $V_R = 10$ V and increases by 1.5 fF when V_R decreases by 20 mV, consistent with the BB837 datasheet. The standard deviation of C_{DUT} is about 0.12 fF at 0.3 Hz measurement bandwidth.[21]

In short, this method can resolve ≲240 ppm variation of a ≃0.5 pF capacitor within a few seconds. Figure 2(d) shows C_{DUT} measured for 72 h, which drifts by <1 fF in 72 h. The variation of C_{DUT} is in good agreement with the room temperature fluctuation, likely introduced by the device itself.

IV. MEASUREMENTS AT MK TEMPERATURE

We install the capacitance setup into an Oxford Triton 400 dilution refrigerator and study the gate-to-2D capacitance of a high-mobility two-dimensional electron gas (2DEG) sample at mK temperature in Fig. 3.[22] The sample consists an $Al_{0.3}Ga_{0.7}As/GaAs/Al_{0.3}Ga_{0.7}As$ quantum well structure grown by molecular beam epitaxy, as illustrated in Fig. 3(a). The 650 Å-wide GaAs quantum well resides 1665 Å below the surface, bound by $Al_{0.3}Ga_{0.7}As$ spacer-layers on both sides. We grow three

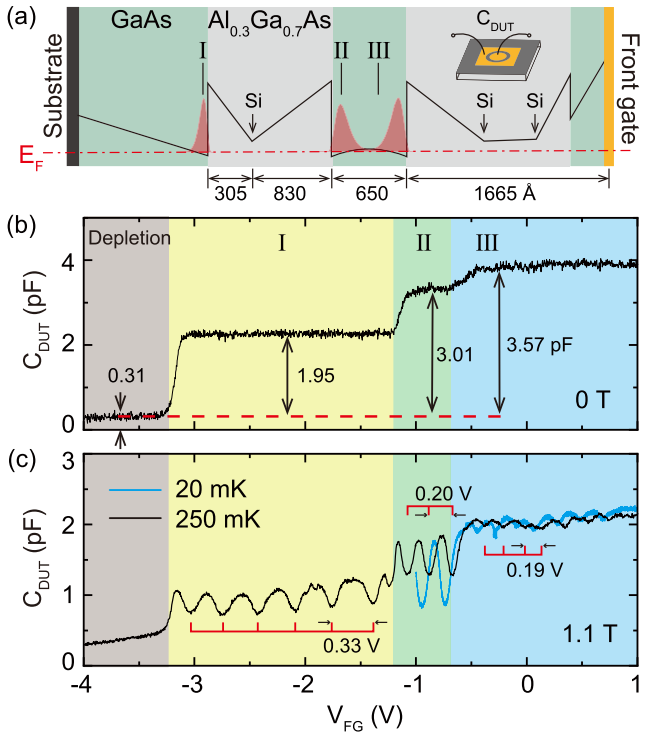

FIG. 3. Studying high-mobility two-dimensional electron gas (2DEG) in GaAs/AlGaAs heterostructure samples with capacitance measurement. (a) Sample structure. Black, green, gray and yellow regions represent the substrate, the GaAs layer, the $Al_{0.3}Ga_{0.7}As$ layer, and the metallic front gate, respectively. The black solid line represents the conduction band edge, and the red dashed-dotted line is the Fermi level E_F. The vertical arrow indicates the δ-doping positions. The red shaded areas represent the charge distribution of 2DEG at zero gate voltage. I, II, and III indicate the effective charge position of the top-most 2DEG in the three cases of (b). The inset is the illustration of the sample. C_{2D} is connected to the bridge by gold wire. (b) The measured capacitance C_{DUT}. The four C_{DUT} plateaus indicate four different working scenarios of the device: depletion and cases I, II, and III. The black double-arrow lines mark the capacitance value for each plateau. (c) C_{DUT} vs V_{FG} at 1.1 T perpendicular magnetic field. The red lines mark the periods of oscillation of the 250 mK trace.

Si-δ-doping-layers in the spacer-layers, two in the surface-side one and one in the substrate-side one. At zero front gate bias, a bilayer-like 2DEG forms inside the quantum well, and another 2DEG forms at the interface between the substrate-side AlGaAs spacer-layer and the GaAs buffer-layer; see Fig. 3(a). The mobility is about 2 $m^2/(V \cdot s)$. We evaporate two concentric gates and measure the gate-to-gate capacitance, i.e., the two gate-to-2D capacitors that are serial-connected by the 2DEG; see the inset in Fig. 3(a). The inner gate radius is 60 μm, and the gap between the two gates is 20 μm. The outer-gate is much bigger than the inner-gate so that C_{DUT} is approximately the inner-gate-to-2D capacitance C_{2D} in parallel with a parasitic capacitance C_p ($C_{DUT} = C_{2D} + C_p$). An isolation capacitor[23] is used between the inner-gate and the bridge so that a DC gate bias V_{FG} can be applied. The frequency and amplitude of V_{in} is 17 MHz and ~0.4 mV_{rms}, respectively. We do not see any increase in the mixing chamber temperature (≲17 mK) when turn on the measurement, evidencing that the heat load at the sample stage is negligible.[22,24]

Figure 3(b) shows C_{DUT} as a function of V_{FG} measured at 250 mK.[25] The electron charging falls into four scenarios, corresponding to the four plateaus seen in Fig. 3(b) data. **Depletion**: The 2DEG under the inner-gate is completely depleted when V_{FG} is small and C_{DUT} is close to zero. **Case I**: As V_{FG} increases, the first 2DEG starts to form at the interface between the buffer-layer and the substrate-side spacer-layer. **Case II**: The second 2DEG forms at the substrate-side interface of the quantum well when V_{FG} reaches −1.20 V. **Case III**: Increasing V_{FG} increases the charge density inside the quantum well as well as makes it more symmetric. The effective charging position becomes close to the quantum well center when electrons starts to fill the second subband, whose charge distribution locates at the surface-side interface of the quantum well.

The 0.31 pF plateau in the depletion region is likely the stray capacitance of the device through the undepleted 2DES between the two gates. We subtract it from the measured capacitance C_{DUT} and summarize the plateau heights corresponding to cases I, II, and III in Table I as C^i_{2D}, $i = 1, 2, 3$ [see also Fig. 3(b)]. Note that C^i_{2D} is inversely proportional to d_i, the distance between the surface and the effective position of the topmost 2DEG.[6] $d_1 \approx 3500$ Å because the effective position of a heterojunction 2DEG is estimated to be ≃50 Å away from the interface.[26] We can calculate d_2 and d_3 and list them in Table I using $[C^i_{2D}]^{-1} \propto \left(\frac{d^i_G}{\varepsilon_G} + \frac{d^i_A}{\varepsilon_A}\right)/\varepsilon_0$, where ε_0 is the vacuum dielectric constant, $\varepsilon_G = 13.18$ ($\varepsilon_A = 12.24$) is the relative dielectric constant of the GaAs ($Al_{0.3}Ga_{0.7}As$) layer, and d^i_G (d^i_A) is the total thickness of the GaAs ($Al_0.3Ga_{0.7}As$) layer in d_i ($= d^i_G + d^i_A$). These results suggest that the effective position of the quantum-well

TABLE I. The parameters of 2DEG obtained from Fig. 3. The subscript $i = 1, 2, 3$ indicates the parameter in cases I, II, and III, respectively.

Cases	C^i_{2D} (pF)	d_i (Å)	V^i_B (V)
I	1.95	3500	0.33
II	3.01	2283	0.20
III	3.57	1906	0.19
I:II:III	1:1.54:1.83	\	1/(1:1.65:1.74)

2DEG is about 32 Å (= 2315 Å−d_2) away from its substrate-side interface when it first appears and moves to 241 Å (=d_3 − 1665 Å) away from its surface-side interface when the electron occupies the second-subband. A comprehensive investigation may track this evolution more thoroughly, which is out of our scope here.

When subjected into a large perpendicular magnetic field B, the electrons of a 2DEG are quenched into discrete Landau levels, leading to density-dependent compressibility. When we tune the 2DEG density by sweeping V_{FG} [see Fig. 3(c)], we observe a C_{DUT} oscillation where each period corresponds to the occupation of two Landau levels (two spins) in the topmost 2DEG.[16] We extracted the oscillation period V_B^i for the three cases and list them in Table I. The reciprocal ratio of V_B^i is similar to the ratio of C_{2D}^i, consistent with our expectation that C_{2D}^i is inversely proportional to V_B^i as $[C_{2D}^i]^{-1} \propto \frac{h}{2e^2} B^{-1} V_B^i$, where h is Planck's constant, e is the electron charge, and B is the magnetic field. Note that the capacitance oscillation is strong in cases I and II but heavily damped in case III. At a lower temperature of 20 mK, the oscillation becomes more pronounced in case II due to the increase of the scattering lifetime but remains roughly unchanged in case III. This is possibly because the two subbands have spatially separated charge distribution, which smooths the compressibility oscillation.

V. CONCLUSION

We have introduced a high-precision, low-excitation capacitance measurement method for 10 mK to room-temperature experiments. We are able to measure the absolute capacitance value using the "V-curve" procedure with <0.1 pF accuracy and monitor the variation of the capacitor using V_{out}. With about 1 mV_{rms} excitation voltage, we can resolve 240 ppm variation of a 500 fF capacitor. We measure the gate-to-2D capacitance of a high-mobility 2DES at mK temperature and extract consistent, essential information of the device. The results demonstrate that our capacitance bridge can detect extremely small capacitance fluctuation with mV-excitation at 10 mK temperature.

ACKNOWLEDGMENTS

Y. Liu acknowledge support from the National Basic Research Program of China (Grant No. 2019YFA0308403) and the National Natural Science Foundation of China (Grant Nos. 92065104 and 12074010) for sample fabrication and measurement. H. Lu acknowledges the support from the National Key R & D Program of China (Grant No. 2018YFA0306200) and the National Natural Science Foundation of China (Grant No. 51732006) for material growth. We thank M. Shayegan, Lloyd Engle, Jianhao Chen, and Xi Lin for valuable discussions.

AUTHOR DECLARATIONS

Conflict of Interest

The authors have no conflicts to disclose.

REFERENCES

[1] M. Kaplit and J. N. Zemel, "Capacitance observations of Landau levels in surface quantization," Phys. Rev. Lett. **21**, 212–215 (1968).
[2] A. M. Voshchenkov and J. N. Zemel, "Admittance studies of surface quantization in [100]-oriented Si metal-oxide-semiconductor field-effect transistors," Phys. Rev. B **9**, 4410–4421 (1974).
[3] T. P. Smith, B. B. Goldberg, P. J. Stiles, and M. Heiblum, "Direct measurement of the density of states of a two-dimensional electron gas," Phys. Rev. B **32**, 2696–2699 (1985).
[4] V. Mosser, D. Weiss, K. v. Klitzing, K. Ploog, and G. Weimann, "Density of states of GaAs-AlGaAs-heterostructures deduced from temperature dependent magnetocapacitance measurements," Solid State Commun. **58**, 5–7 (1986).
[5] R. C. Ashoori, H. L. Stormer, J. S. Weiner, L. N. Pfeiffer, S. J. Pearton, K. W. Baldwin, and K. W. West, "Single-electron capacitance spectroscopy of discrete quantum levels," Phys. Rev. Lett. **68**, 3088–3091 (1992).
[6] J. Jo, E. A. Garcia, K. M. Abkemeier, M. B. Santos, and M. Shayegan, "Probing the subband structure of a wide electron system in a parabolic quantum well via capacitance-voltage measurements," Phys. Rev. B **47**, 4056–4059 (1993).
[7] J. P. Eisenstein, L. N. Pfeiffer, and K. W. West, "Compressibility of the two-dimensional electron gas: Measurements of the zero-field exchange energy and fractional quantum Hall gap," Phys. Rev. B **50**, 1760–1778 (1994).
[8] T. P. Smith, W. I. Wang, and P. J. Stiles, "Two-dimensional density of states in the extreme quantum limit," Phys. Rev. B **34**, 2995–2998 (1986).
[9] M. J. Yang, C. H. Yang, B. R. Bennett, and B. V. Shanabrook, "Evidence of a hybridization gap in 'semimetallic' InAs/GaSb systems," Phys. Rev. Lett. **78**, 4613–4616 (1997).
[10] B. M. Hunt, J. I. A. Li, A. A. Zibrov, L. Wang, T. Taniguchi, K. Watanabe, J. Hone, C. R. Dean, M. Zaletel, R. C. Ashoori, and A. F. Young, "Direct measurement of discrete valley and orbital quantum numbers in bilayer graphene," Nat. Commun. **8**, 948 (2017).
[11] S. L. Tomarken, Y. Cao, A. Demir, K. Watanabe, T. Taniguchi, P. Jarillo-Herrero, and R. C. Ashoori, "Electronic compressibility of magic-angle graphene superlattices," Phys. Rev. Lett. **123**, 046601 (2019).
[12] J. P. Eisenstein, L. N. Pfeiffer, and K. W. West, "Negative compressibility of interacting two-dimensional electron and quasiparticle gases," Phys. Rev. Lett. **68**, 674–677 (1992).
[13] A. A. Zibrov, C. Kometter, H. Zhou, E. M. Spanton, T. Taniguchi, K. Watanabe, M. P. Zaletel, and A. F. Young, "Tunable interacting composite fermion phases in a half-filled bilayer-graphene Landau level," Nature **549**, 360–364 (2017).
[14] A. A. Zibrov, P. Rao, C. Kometter, E. M. Spanton, J. I. A. Li, C. R. Dean, T. Taniguchi, K. Watanabe, M. Serbyn, and A. F. Young, "Emergent Dirac gullies and gully-symmetry-breaking quantum Hall states in *ABA* trilayer graphene," Phys. Rev. Lett. **121**, 167601 (2018).
[15] H. Deng, L. N. Pfeiffer, K. W. West, K. W. Baldwin, L. W. Engel, and M. Shayegan, "Probing the melting of a two-dimensional quantum Wigner crystal via its screening efficiency," Phys. Rev. Lett. **122**, 116601 (2019).
[16] H. Irie, T. Akiho, and K. Muraki, "Determination of g-factor in InAs two-dimensional electron system by capacitance spectroscopy," Appl. Phys. Express **12**, 063004 (2019).
[17] A. Hazeghi, J. A. Sulpizio, G. Diankov, D. Goldhaber-Gordon, and H. S. P. Wong, "An integrated capacitance bridge for high-resolution, wide temperature range quantum capacitance measurements," Rev. Sci. Instrum. **82**, 053904 (2011).
[18] G. J. Verbiest, H. Janssen, D. Xu, X. Ge, M. Goldsche, J. Sonntag, T. Khodkov, L. Banszerus, N. von den Driesch, D. Buca, K. Watanabe, T. Taniguchi, and C. Stampfer, "Integrated impedance bridge for absolute capacitance measurements at cryogenic temperatures and finite magnetic fields," Rev. Sci. Instrum. **90**, 084706 (2019).
[19] In Fig. 2(a), CDUT slightly deviates from Cnom when $C_{DUT} \neq C_{ref}$. This is not surprising because the bridge output is less sensitive to C_{DUT} in this case so that the leaking signal causes more deviation. The accuracy is mainly dominated by the parasitic capacitance. We carefully shield the signal with coaxial cables and optimize the sample stage so that the parasitic capacitance is $\lesssim$0.1 pF, evidenced by the error bar in Fig. 2(a). Although parasitic capacitance cannot be eliminated, its variation between different measurements is even smaller $\delta(C_p) \sim 0.01$ pF.[24]

Therefore, we can measure absolute capacitance with an accuracy up to <0.1 pF once we carefully calibrate the setup with a procedure similar to Fig. 2(a).

[20]Note that Eq. (2) only works at the vicinity of the balance point. When $\frac{1}{\omega C_{\mathrm{DUT}}}, \frac{1}{\omega C_{\mathrm{ref}}} \gg R_{\mathrm{ref}}, R_{\mathrm{h}}, R_0$, the complete expression is $V_{\mathrm{out}} \simeq G \cdot \left(\frac{R_{\mathrm{in}}}{\frac{1}{j\omega C_{\mathrm{DUT}}}+R_{\mathrm{in}}} \cdot \frac{R_{\mathrm{ref}}}{R_{\mathrm{ref}}+R_{\mathrm{h}}} - \frac{R_{\mathrm{in}}}{\frac{1}{j\omega C_{\mathrm{ref}}}+R_{\mathrm{in}}} \cdot \frac{R_{\mathrm{h}}}{R_{\mathrm{ref}}+R_{\mathrm{h}}} \right) \cdot V_{\mathrm{in}}$,,, where G is the total gain of the amplifier/mixer and $R_{\mathrm{in}} \simeq 50\ \Omega$ is the input impedance of the preamplifier. When measured by the "V-curve" procedure, the bridge can be divided into two cases: (a) when $R_{\mathrm{ref}} \gg R_{\mathrm{h}}$ ($R_{\mathrm{ref}} \ll R_{\mathrm{h}}$), $V_{\mathrm{out}} \simeq j\omega C_{\mathrm{DUT}} R_{\mathrm{in}} G V_{\mathrm{in}}$ ($-j\omega C_{\mathrm{ref}} R_{\mathrm{in}} G V_{\mathrm{in}}$); (b) when $R_{\mathrm{ref}} \sim R_{\mathrm{h}}$, $\partial V_{\mathrm{X}}/\partial\left(\frac{R_{\mathrm{h}}}{R_{\mathrm{ref}}+R_{\mathrm{h}}}\right) \simeq \mathrm{Im}\left(-\frac{R_{\mathrm{in}}}{\frac{1}{j\omega C_{\mathrm{ref}}}+R_{\mathrm{in}}}\right) \cdot G V_{\mathrm{in}}$ [shown in Fig. 1(b)]. At the vicinity of the balance point, where $\frac{C_{\mathrm{DUT}}}{C_{\mathrm{ref}}} \approx \frac{R_{\mathrm{h}}}{R_{\mathrm{ref}}}$, $\partial V_{\mathrm{X}}/\partial\left(\frac{C_{\mathrm{DUT}}}{C_{\mathrm{ref}}+C_{\mathrm{DUT}}}\right) \simeq \mathrm{Im}\left(\frac{R_{\mathrm{in}}}{\frac{1}{j\omega C_{\mathrm{ref}}}+R_{\mathrm{in}}}\right) \cdot G V_{\mathrm{in}}$, and we reach the approximation equation (2).

[21]The equivalent voltage noise of the whole setup at the input of the RF preamplifier has a spectrum density of about 8 $\mathrm{nV}/\sqrt{\mathrm{Hz}}$.

[22]The mixing chamber temperature increases from ≃8 to ≃17 mK after we install three semi-rigid coaxial cables. In a separate report, we use extra-thin flexible coaxial wires and the mixing chamber temperature can be kept below 10 mK during the measurement.[24]

[23]The isolation capacitor is 22 nF in this measurement, which needs to be much larger than the device capacitance.

[24]L. Zhao, W. Lin, Y. J. Chung, K. W. Baldwin, L. N. Pfeiffer, and Y. Liu, "Capacitive response of Wigner crystals at the quantum Hall plateau," arXiv:2201.06203 (2022).

[25]In this paper, all quoted temperatures are mixture chamber plate temperatures of the dilution refrigerator.

[26]T. Ando, A. B. Fowler, and F. Stern, "Electronic properties of two-dimensional systems," Rev. Mod. Phys. **54**, 437–672 (1982).